Journal of Solid State Chemistry 182 (2009) 3138–3142

Contents lists available at ScienceDirect

Journal of Solid State Chemistry

journal homepage: www.elsevier.com/locate/jssc

Fabrication and thermoelectric properties of fine-grained TiNiSn compounds

Minmin Zou [a], Jing-Feng Li [a,*], Bing Du [a], Dawei Liu [a], Takuji Kita [b]

[a] State Key Laboratory of New Ceramics and Fine Processing, Department of Materials Science and Engineering, Tsinghua University, Beijing 100084, China
[b] Advanced Material Engineering Division, Vehicle Engineering Group, Higashifuji Technical Center, Toyota Motor Corporation, 1200, Mishuku, Susono, Shizuoka 410-1193, Japan

ARTICLE INFO

Article history:
Received 22 May 2009
Received in revised form
28 August 2009
Accepted 5 September 2009
Available online 11 September 2009

Keywords:
Thermoelectric material
Half-Heusler compound
Mechanical alloying
Spark plasma sintering

ABSTRACT

Nearly single-phased TiNiSn half-Heusler compound thermoelectric materials were synthesized by combining mechanical alloying (MA) and spark plasma sintering (SPS) in order to reduce its thermal conductivity by refining the grain sizes. Although TiNiSn compound powders were not synthesized directly via MA, dense bulk samples of TiNiSn compound were obtained by the subsequent SPS treatment. It was found that an excessive Ti addition relative to the TiNiSn stoichiometry is effective in increasing the phase purity of TiNiSn half-Heusler phase in the bulk samples, by compensating for the Ti loss caused by the oxidation of Ti powders and MA processing. The maximum power factor value obtained in the Ti-compensated sample is 1720 $\mu W\,m^{-1}\,K^{-2}$ at 685 K. A relatively high ZT value of 0.32 is achieved at 785 K for the present undoped TiNiSn compound polycrystals.

1. Introduction

Thermoelectric materials have received great attention in recent years because of their promising applications of electronic refrigeration and power generation. The energy conversion efficiency of a thermoelectric device is mainly determined by the dimensionless figure of merit (ZT) of its corresponding thermoelectric materials. ZT is expressed as $ZT=\alpha^2T/\rho\kappa$, where T is the absolute temperature, α is the Seebeck coefficient or thermopower, ρ is the electrical resistivity, and κ is the thermal conductivity. Good thermoelectric materials should have large ZT values, which require high α but low ρ and κ.

Ternary half-Heusler compounds MNiSn (M=Ti, Zr, Hf) have a cubic MgAgAs-type structure with a space group of $F\bar{4}3m$. These compounds show promising thermoelectric properties because of their narrow band gap [1–5], about 0.1–0.2 eV at the Fermi level. These alloys exhibit high Seebeck coefficient and low electrical resistivity. For example, Bhattacharya et al. obtained a high power factor ($PF=\alpha^2/\rho$) up to 6150 $\mu W\,m^{-1}\,K^{-2}$ at 650 K in a sample of $TiNiSn_{0.95}Sb_{0.05}$ [6], showing that the TiNiSn-based half-Heusler alloys have a great potential as a mediate-temperature thermoelectric material. It is well known that undoped MNiSn compounds usually have low ZT values about 0.005–0.01 at room temperature [7]. Through doping, ZT values reach 0.7 and 0.78 for the composition $Zr_{0.5}Hf_{0.5}Ni_{0.8}Pd_{0.2}Sn_{0.99}Sb_{0.01}$ at 800 K and $Ti_{0.95}Hf_{0.05}NiSn_{0.99}Sb_{0.01}$ at 770 K as reported by Shen et al. [8] and Kim et al. [9], respectively. Even an extremely high ZT value of 1.5 at 700 K was reported for the composition $(Zr_{0.5}Hf_{0.5})_{0.5}Ti_{0.5}NiSn_{0.998}Sb_{0.002}$ [10].

However, a dominant drawback of this material is their high lattice thermal conductivity (κ_L), which is as high as 10 W/m K at room temperature [7]. Researchers have done lots of work to reduce the thermal conductivity by isoelectronic alloying and atomic substitution. Shen et al. [8] reported the values of κ=2 W/m K at 800 K in a sample of $Zr_{0.5}Hf_{0.5}Ni_{0.5}Pd_{0.5}Sn_{0.99}Sb_{0.01}$ and κ=3 W/m K in the sample $Zr_{0.5}Hf_{0.5}Ni_{0.8}Pd_{0.2}Sn_{0.99}Sb_{0.01}$. It is obvious that their compositions are complex. In addition, these materials are usually fabricated by arc melting which often causes compositional segregation. Although the compositional segregation can be reduced by long time annealing, the microstructure usually has coarse grains characteristic of the melting process [11–13]. Goldsmid et al. [14] presented a concept of reducing room temperature thermal conductivity by grain boundary scattering in the half-Heusler system, in other words, reducing grain size to decrease κ_L. Bhattacharya et al. [11,12] also reported that boundary scattering can affect the thermal conductivity of half-Heusler alloys. Some researchers tried a process to grind arc-melted bulks to fine powders then use hot pressing to produce fine-grained materials, but such a route complicated the fabrication process [9,10].

Recently, the combination of MA and SPS was widely used to synthesize thermoelectric materials, such as Bi_2Te_3 [15,16], $CoSb_3$ [17] and $AgPb_mSbTe_{2+m}$ systems [18,19]. This method is useful to avoid compositional segregation and coarse grains. The fine-grained materials obtained in this way are favorable for thermoelectric applications because of the reduced thermal conductivity caused by grain boundary scattering. In addition, MA is also an effective method to fabricate the compound that is composed by

* Corresponding author. Fax: +86 10 62771160.
E-mail address: jingfeng@mail.tsinghua.edu.cn (J.-F. Li).

0022-4596/$ - see front matter © 2009 Elsevier Inc. All rights reserved.
doi:10.1016/j.jssc.2009.09.003

elements with significantly different melting points [20]. For TiNiSn compound, the great difference of melting points between Sn and the other two elements increases the processing complexity for the traditional melting techniques. In this work, the combination of MA and SPS was applied to synthesize TiNiSn half-Heusler compounds. The thermoelectric properties were investigated in the temperature range from 300 to 900 K.

2. Experimental procedure

Starting materials were highly pure powders of titanium (99.99%), nickel (99.99%) and tin (99.99%). The powder mixtures at the determined ratios were milled in a planetary mill (Pulveristte 6, Germany) at 300 rpm under the protection of Ar atmosphere, using zirconia-lined vial and zirconia ball. Obtained powders were sintered by SPS in a graphite die at a heating rate of 100 K/min and with a soaking duration of 10 min.

The phase structures of the MA-treated powders and the SPSed bulk materials were investigated by X-ray diffraction (XRD, D/max-2500) using Cu$K\alpha$ radiation. The compositions were measured by inductive coupled plasma emission spectrometer (ICP, IRIS Intrepid II XSP) and energy-dispersive X-ray spectroscopy (EDS). The microstructure was analyzed by transmission electron microscopy (TEM, JEM-2011). Seebeck coefficient and electrical resistivity were measured simultaneously by a Seebeck coefficient/electric resistance measuring system (ZEM-2, Ulvac-Riko, Japan). The thermal conductivity was calculated from the thermal diffusivity (D), the heat capacity (C_p) and the density (d) according to the relationship $\kappa = D \times C_p \times d$. The thermal diffusivity was measured by the laser flash method (TC-9000, Ulvac-Riko, Japan). Both the laser flash method and the differential scanning calorimeter (DSC-60, Shimadzu, Japan) were used to measure the heat capacity, while the density was measured by the Archimedes method.

3. Results and discussion

Although TiNiSn compound powders were not synthesized directly by MA, it was found that the MA treatment enhanced the reaction of forming TiNiSn compounds during SPS. Fig. 1 shows the XRD patterns of the raw materials, the powder mixture after MA (2.5 h) and the corresponding bulk sample after SPS (1073 K), respectively. In comparison with the powder mixture before MA, the component phases of the powder changed dramatically after MA for 2.5 h. A compound identified as Ni_3Sn_4 (PDF#65-4310) was detected in the powder mixture subjected to MA for 2.5 h except for Ti and Ni. From the previous study [21], it is known that TiNiSn compound still cannot be synthesized when the milling time was prolonged to 20 h. It seems that the giant difference of melting points between Sn and the other two elements is not favorable for the formation of TiNiSn via MA. After SPS, TiNiSn compound was synthesized with a few amounts of $TiNi_2Sn$ and $Ni_{3.39}Sn_4$, suggesting that the amount of Ti element is deficient to form TiNiSn completely basing on the element equal principle. Therefore, excessive Ti was added to the initial composition, thus the starting composition can be written as $Ti_{1+x}NiSn$ (x=0.0–0.6).

Fig. 2 shows the XRD patterns of the samples with different initial compositions sintered at 1073 and 1123 K. It can be seen that diffraction peaks of impurity phases vanished gradually with increasing Ti contents. Nearly single-phased TiNiSn compound was synthesized when x=0.4, in which the amounts of $TiNi_2Sn$ and $Ni_{3.39}Sn_4$ were almost negligible. The presence of impurity phase might be caused by insufficient reaction time for the SPS process. Another impurity phase appeared when x value is over 0.4, which is identified to be Ti_3Sn (PDF#06-0583). It is obvious

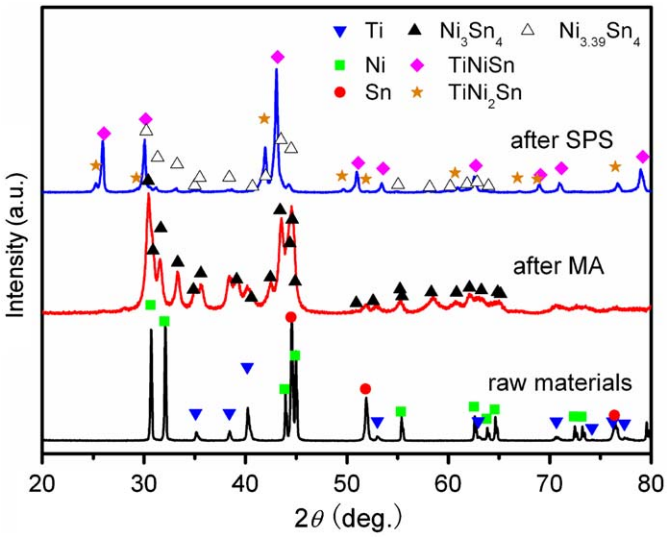

Fig. 1. XRD patterns of the raw materials, the powder mixture after MA (2.5 h) and the bulk sample after SPS (1073 K).

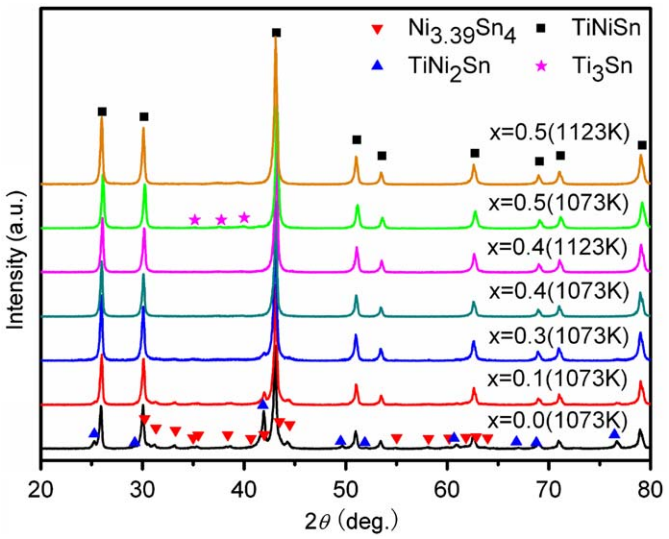

Fig. 2. XRD patterns of the samples $Ti_{1+x}NiSn$ (x=0.0–0.5) sintered at 1073 and 1123 K. It is worth noting that the molecular formula $Ti_{1+x}NiSn$ represents the starting composition of the samples, not the actual composition.

that x=0.4 is the optimal Ti content for the synthesis of TiNiSn compound by the present method.

Fig. 3(a) shows a typical TEM micrograph for the sample with the initial composition $Ti_{1.4}NiSn$ sintered at 1123 K. The relatively large grain is TiNiSn phase, whose average grain size is ~200–400 nm. The grain size is smaller than that of most bulk materials synthesized by the melting method, and the grain refinement is favorable for reducing lattice thermal conductivity. A bright crescent grain was observed at the grain boundary, in which only Ti and O elements were detected by EDS and their ratio (Ti:O) agreed well with 1:2, so this crescent grain was determined to be TiO_2 (Fig. 3(b)). It is worth noting that the presence of TiO_2 particle is not a specific situation but a general case, which was frequently found all over the TEM sample. We can infer that although MA is carried out in an Ar atmosphere, the remnant oxygen in the jar is difficult to be totally eliminated. Therefore, the oxidation of Ti could not completely avoid.

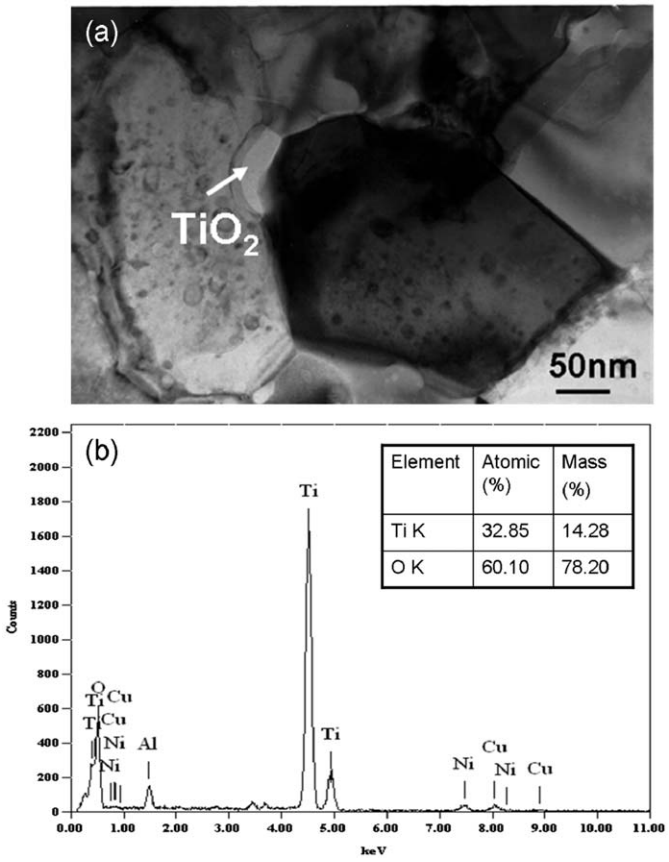

Fig. 3. (a) TEM image of the sample $Ti_{1.4}NiSn$ (1123 K). (b) EDS pattern of the TiO_2 particle.

Table 1
ICP results of MA-derived powder (2.5 h) and the SPSed sample $Ti_{1.4}NiSn$ (1123 K).

Element	Initial composition (atomic ratio)	MAed powder (atomic ratio)	SPSed sample (atomic ratio)
Ti	1.40	1.18	1.23
Ni	1.00	1.00	1.00
Sn	1.00	0.97	1.01

The precise compositions of the MA-treated powder and the SPSed sample for $x=0.4$ are exhibited in Table 1. The content of Ti decreased sharply after MA, while the atom ratio did not change much after SPS, suggesting that the element volatilization during SPS was not serious. Because of the confirmed existence of TiO_2 particles, we can infer that oxidization may be one possible reason for the Ti loss. Nevertheless, the nano TiO_2 particles may be useful to reduce the thermal conductivity through accurate control. In fact, recently, oxide nanoparticles are intentionally introduced into $CoSb_3$-based thermoelectric materials to reduce its thermal conductivity [22]. Moreover, another interesting phenomenon was observed during MA: Ti powders were much easier to adhere to the vial and ball than the other two powders, thus the Ti element was not sufficient to react with Ni and Ni_3Sn_4 to form TiNiSn. Hence, the adhesion of Ti may be another possible reason for the Ti loss.

Fig. 4(a) shows the temperature dependence of electrical resistivity for all the samples. The electrical resistivity is relatively low, being about 5–20 μΩm near room temperature for the present undoped TiNiSn compounds. For the samples sintered at 1073 K, the electrical resistivity increases with increasing x up to $x=0.5$, then decreases with further increasing x, suggesting a close relationship between the resistivity and the phase purity. When $x<0.3$, the electrical resistivity is low and nearly temperature-independent because of their low phase purity, with a large amount of metallic phase. The electrical resistivity decreases with temperature, being indicative of semiconductors, when the x value exceeds 0.4.

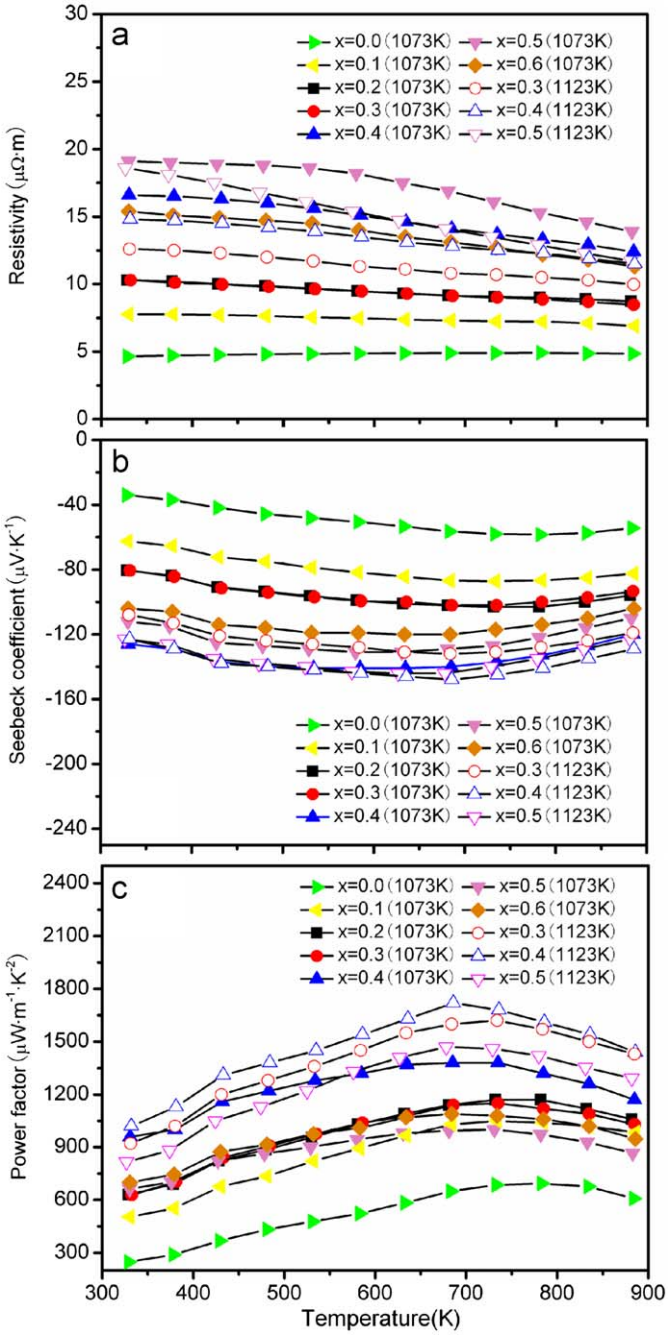

Fig. 4. Temperature dependence of electrical resistivity (a), Seebeck coefficient (b) and power factor (c) of $Ti_{1+x}NiSn$ ($x=0.0$–0.6) sintered at 1073 and 1123 K.

Fig. 4(b) shows the temperature dependence of Seebeck coefficient. The Seebeck coefficient is negative, suggesting that all samples are n-type. For each sample, there are two distinct regions with different behaviors. Absolute Seebeck coefficient, $|\alpha|$,

increases as temperature increases from room temperature and reaches a maximum at ~700 K, then starts to decrease with further increasing temperature. This is due to the excitation of electron–hole pairs across the energy gap, and the opposite contribution to α from the two carriers reduces the observed $|\alpha|$. For the samples sintered at 1073 K, the Seebeck coefficient increases with increasing x value and then decreases with further increasing x value, being consistent with the tendency of electrical resistivity. The Seebeck coefficient of the samples sintered at 1123 K is higher than that sintered at 1073 K, indicating that 1123 K is a better sintering temperature for the synthesis of TiNiSn by the present process. The maximum Seebeck coefficient value is $-148\ \mu V/K$ for the sample with $x=0.4$ sintered at 1123 K. This relatively small Seebeck coefficient, compared with other literature data [7,9,23], may be attributed to the high carrier concentration caused by some residual impurity phases. As suggested by Uher et al. [24], the measured Seebeck coefficient significantly depends on the synthesis process. For example, as the annealing time increases, the amount of the secondary phases decreases, leading to a larger Seebeck coefficient. The fabrication method without long-time annealing, usually leads to small grain size but low Seebeck coefficient. For instance, $Ti_{1-x}(Hf_{0.919}Zr_{0.081})_xNiSn$, prepared by solid reaction and SPS, reported by Tang et al. [25] also shows a small Seebeck coefficient.

The power factor is calculated from the measured Seebeck coefficient and electrical resistivity and the results are shown in Fig. 4(c). The power factor of the samples sintered at 1123 K is generally larger than that of samples sintered at 1023 K owing to their higher phase purity. The power factor also exhibits an apparent tendency like the electrical resistivity and the Seebeck coefficient: firstly increases with increasing x, and then decreases with further x increase when x is over 0.4, indicating the close relationship between thermoelectric properties and phase purity. We can conclude that the phase purity is related not only to SPS temperature but also to x value. The maximum power factor value is $1720\ \mu W\ m^{-1}\ K^{-2}$ at 685 K for the sample with $x=0.4$ sintered at 1123 K.

Fig. 5 describes the thermal diffusivity of the samples sintered at 1123 K with $x=0.3$–0.5 (solid line) and the thermal conductivity of the sample $Ti_{1.4}NiSn$ (1123 K) indicated by the dash line. As shown in Fig. 5, all the three samples have similar thermal diffusivity values, which are in the range of 1.3–1.9 mm^2/s. Heat capacity measured by the laser flash method and the differential scanning calorimeter are shown in the inset of Fig. 5. The two curves are consistent with each other, in which the heat capacity

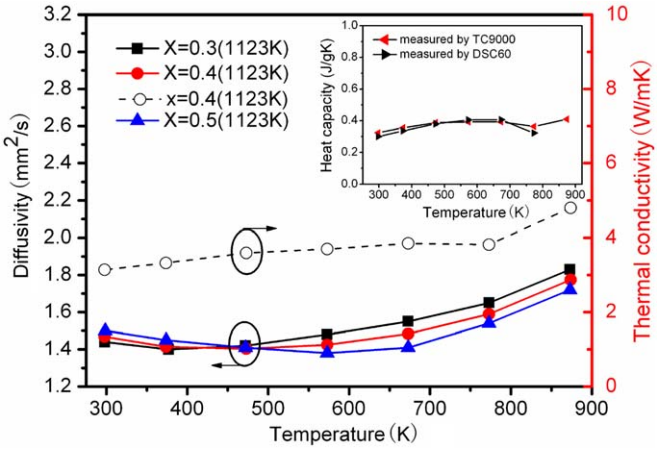

Fig. 5. Temperature dependence of thermal diffusivity for the samples sintered at 1123 K with $x=0.3$–0.5 and thermal conductivity of the sample $Ti_{1.4}NiSn$ (1123 K).

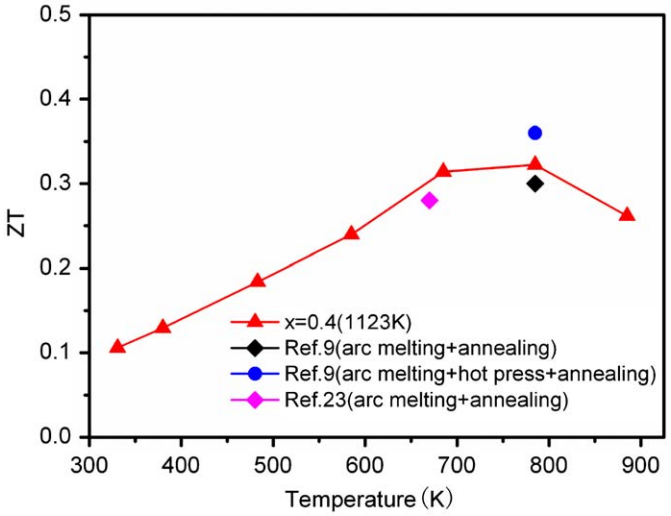

Fig. 6. Temperature dependence of the dimensionless figure of merit (ZT) of the sample $Ti_{1.4}NiSn$ (1123 K).

is 0.32 J/g K at room temperature. The measured density value of the sample $Ti_{1.4}NiSn$ (1123 K) is 6.61 g/cm^3. With the measured thermal diffusivity, density and the heat capacity measured by the laser flash method, the thermal conductivity of the sample $Ti_{1.4}NiSn$ (1123 K) is also displayed in Fig. 5. It can be seen that its thermal conductivity increases slightly with increasing temperature. The minimum thermal conductivity is about 3.14 W/m K at room temperature, which is a very low value for the MNiSn alloys. It is well known that the thermal conductivity is comprised of the lattice thermal conductivity (κ_L) and the electron thermal conductivity (κ_E). The κ_E of the sample $Ti_{1.4}NiSn$ (1123 K) at room temperature is calculated to be 0.44 W/m K by the Wiedemann–Franz law. The estimated κ_L is as low as 2.7 W/m K, which is due to the strong grain boundary scattering caused by the fine grains.

The dimensionless figure of merit, ZT, of the sample $Ti_{1.4}NiSn$ (1123 K) is shown in Fig. 6. A relatively high ZT value of 0.32 was obtained at 785 K mainly due to the reduced thermal conductivity. This ZT value is comparable with the recorded value obtained in other undoped TiNiSn compounds reported in the literatures [9,23]. As above mentioned, previously the TiNiSn-based compounds were synthesized by arc melting, for which a long time annealing process was needed to reduce the contents of impurity phases, but the present process is more easy and productive. A further study is in progress to enhance the ZT value by elemental substitutions to Ti and/or Sn sites.

4. Conclusions

The present study confirmed that the combined process of MA and SPS is applicable to the synthesis of the TiNiSn-based half-Heusler thermoelectric materials. Almost single-phased TiNiSn-based compounds were prepared by taking measures to compensate for the Ti loss during the MA and SPS processes. The resultant materials show dense and uniform microstructure with small grains of about 200–400 nm in diameter. Because of the refined grain sizes compared with the previous arc melting process, the thermal conductivity of the present samples with the highest phase purity was reduced to as low as 3.14 W/m K at room temperature. As a result, a relatively high ZT value of 0.32 was obtained at 785 K for the present undoped TiNiSn compounds.

Acknowledgments

The authors acknowledge financial support from the National Basic Research Program of China (Grant no. 2007CB607500) and Tsinghua-Toyota Collaborative Research Project (no. 0307J36) as well as National Nature Science Foundation (Grants no. 50820145203).

References

[1] F.G. Aliev, N.B. Brandt, V.V. Moschalkov, V.V. Kozyrkov, R.V. Skolozdra, A.I. Belogorokhov, Z. Phys. B Condens. Matter 75 (1989) 167–171.
[2] F.G. Aliev, Physica B 171 (1991) 199–205.
[3] S. Öğüt, K.M. Rabe, Phys. Rev. B 51 (1995) 10443–10453.
[4] J. Tobola, J. Pierre, J. Alloys Compd. 296 (2000) 243–252.
[5] P. Larson, S.D. Mahanti, M.G. Kanatzidis, Phys. Rev. B 62 (2000) 12754–12762.
[6] S. Bhattacharya, A.L. Pope, R.T. Littleton IV, T.M. Tritt, V. Ponnambalam, Y. Xia, S.J. Poon, Appl. Phys. Lett. 77 (2000) 2476–2478.
[7] H. Hohl, A.P. Ramirez, C. Goldmann, G. Ernst, B. Wölfing, E. Bucher, J. Phys. Condens. Matter 11 (1999) 1697–1709.
[8] Q. Shen, L. Chen, T. Goto, T. Hirai, J. Yang, G.P. Meisner, C. Uher, Appl. Phys. Lett. 79 (2001) 4165–4167.
[9] S.W. Kim, Y. Kimura, Y. Mishima, Intermetallics 15 (2007) 349–356.
[10] N. Shutoh, S. Sakurada, J. Alloys Compd. 389 (2005) 204–208.
[11] S. Bhattacharya, T.M. Tritt, Y. Xia, V. Ponnambalam, S.J. Poon, N. Thadhani, Appl. Phys. Lett. 81 (2002) 43–45.
[12] S. Bhattacharya, M.J. Skove, M. Russell, T.M. Tritt, Y. Xia, V. Ponnambalam, S.J. Poon, N. Thadhani, Phys. Rev. B 77 (2008) 184203-1–184203-8.
[13] K. Kurosaki, T. Maekawa, H. Muta, S. Yamanaka, J. Alloys Compd. 397 (2005) 296–299.
[14] J.W. Sharp, S.J. Poon, H.J. Goldsmid, Phys. Status Solidi A 187 (2001) 507–516.
[15] J.-F. Li, J. Liu, Phys. Status Solidi A 203 (2006) 3768–3773.
[16] L.-D. Zhao, B.-P. Zhang, J.-F. Li, M. Zhou, W.-S. Liu, J. Liu, J. Alloys Compd. 455 (2008) 259–264.
[17] W.S. Liu, B.P. Zhang, J.-F. Li, H. Wang, Key Eng. Mater. 834 (2007) 336–338.
[18] H. Wang, J.-F. Li, C.-W. Nan, M. Zhou, W.S. Liu, B.-P. Zhang, T. Kita, Appl. Phys. Lett. 88 (2006) 092104-1–092104-3.
[19] M. Zhou, J.-F. Li, T. Kita, J. Am. Chem. Soc. 130 (2008) 4527–4532.
[20] L.-D. Zhao, B.-P. Zhang, W.-S. Liu, H.-L. Zhang, J.-F. Li, J. Solid State Chem. 181 (2008) 3278–3282.
[21] M.M. Zou, J.-F. Li, Rare Metal Mater. Eng., in press.
[22] X.Y. Zhao, X. Shi, L.D. Chen, W.Q. Zhang, S.Q. Bai, Y.Z. Pei, X.Y. Li, T. Goto, Appl. Phys. Lett. 89 (2006) 092121-1–092121-3.
[23] T. Katayama, S.W. Kim, Y. Kimura, Y. Mishima, J. Electron. Mater. 32 (2003) 1160–1165.
[24] C. Uher, J. Yang, S. Hu, D.T. Morelli, G.P. Meisner, Phys. Rev. B (1999) 8615–8621.
[25] H.Q. Liu, X.F. Tang, K. Wang, C. Song, Q.J. Zhang, Acta Phys. Sin. 55 (2006) 2003–2007.